Evaluation of the convergent properties of the Linear Matching Method for computing the collapse of structural components

O. Barrera, A.C.F. Cocks, A.R.S. Ponter

Evaluation of the convergent properties of the Linear Matching Method for computing the collapse of structural components

O. Barrera, A.C.F. Cocks, A.R.S. Ponter

PII: S0997-7538(09)00027-8
DOI: 10.1016/j.euromechsol.2009.02.007
Reference: EJMSOL 2503

To appear in: *European Journal of Mechanics A/Solids*

Received date: 7 November 2008
Accepted date: 13 February 2009

Please cite this article as: O. Barrera, A.C.F. Cocks, A.R.S. Ponter, Evaluation of the convergent properties of the Linear Matching Method for computing the collapse of structural components, *European Journal of Mechanics A/Solids* (2009), doi: 10.1016/j.euromechsol.2009.02.007

Evaluation of the Convergent Properties of the Linear Matching Method for Computing the Collapse of Structural Components.

O. Barrera [*] **, A.C.F. Cocks** [°] **and A.R.S. Ponter** [⊕]

[*] *Department DASTEC University "Mediterranea" of Reggio Calabria, Via Melissari Feo di Vito, I-89124 Reggio Calabria, IT*

[°] *Department of Engineering Science University of Oxford, Parks Road, Oxford OX1 3PJ, UK*

[⊕] *Department of Engineering University of Leicester, University Road, Leicester LEI 7RH, UK*

ABSTRACT

The paper considers the application of the Linear Matching method to the limit analysis of perfectly plastic portal frames. This allows the display of the characteristic features of this method to a class of structural problems that have been studied by several other methods. The convergence of both upper and lower bounds is proven and a simple geometric interpretation displays the nature of the programming method. Through a sequence of examples the convergence properties of the method are displayed, showing that complete convergence can sometimes be delayed by the proximity of mechanisms with near equal limit loads.

Keywords: Limit analysis; Linear Matching Method; Convergence; Collapse mechanism.

---

1. INTRODUCTION

The development of numerical methods for the evaluation of limits in classical plasticity theory has a long history with a number of significant strands. The upper and lower bound theorems of limit and shakedown analysis naturally lend themselves to programming methods, both linear and non-linear, producing, today, efficient solution procedures (Weichert and Maier, 2001). Recently, the application of mathematical programming methods to the limit analysis of portal frames has been consolidated and summarised by Cocchetti and Maier (2003). These methods have also been extended to the behaviour of elastic-softening plastic portal frames, emphasing the importance of Mathematical Programming with Equilibrium Constraints (MPEC) methods by Ferris and Tin-Loi (2001) and Tangaramvong and Tin-Loi (2007, 2008). MPEC methods correspond to a class of methods that may be applied to structural mechanics problems and problems in business and finance. There has always existed a strong cross fertilization between mathematical programming methods in applied mechanics and in other applications. It is, therefore, beneficial to display new methods in applied mechanics in a form that allows a direct comparison with existing mathematical programming methods and the problem of the portal frame provides a useful vehicle in this respect, as well as being a significant problem in structural design.

In recent times, an alternative approach to classical plasticity problems has been developed, motivated by a desire to calculate classical plasticity limits using conventional finite element methods as the basis for iterative procedures. Marriot (1985)

has discussed the Modulus Variation Procedures (MVP) that generates lower bounds within some kinematic contexts by representing an elastic-plastic stress field as the solution of a linear problem with spatially varying moduli. Related design orientated methods have been discussed by Seshadri and Fernando (1993) and Mackenzie and Boyle (1993). These methods have been devised with structural design in mind. Whereas programming methods have a well defined theoretical structure where convergence can be meaningfully discussed, generally MVP and related methods have been treated in a more ad-hoc manner and have proved to give a rather variable performance. Recently, Marin-Artieda and Dargush (2007) describe the application of these methods to portal frames and demonstrate both the strength (simplicity) and weakness (uncertainty over convergence) of this class of methods when applied to the simplest of the plasticity problems, limit analysis. They conclude that the original method of Marriot (1985) provides the most satisfactory lower bound solutions but rarely the exact limit state solution.

A further branch of these developments, the Linear Matching Methods (LMM) (Ponter et al, 2000 and Ponter and Engelhardt, 2000), arises from the same general approach of MVP methods, the use of standard linear finite element analysis with spatially varying moduli, but with the objective of defining programming methods with very well defined convergence properties. By this means, methods are derived with the sound theoretical foundation of programming methods and the simplicity of MVP. The primary motivation has been the development of methods that may be used as a computational tool for the UK Life Assessment Method R5 (Ainsworth, 1997) where thermo-mechanical loading for complex continuum structures is the primary concern. For this range of problems, methods have been derived for limit, shakedown and ratchet limits and a number of extensions allow for high temperature creep behaviour (Chen. et al, 2006 a,b). In all this work, the upper bound, kinematic, aspect of the method has been emphasised and, indeed, there is evidence that it may not be possible to derive a convergent method of this type that relies only on the lower bound theorems of plasticity (Ponter, 2007). However, amongst the published work on these methods, there is the lack of a straightforward description of the Linear Matching Method and its convergence properties within an easily understood structural context. The work of Marin-Artieda and Dargush (2007) provides an opportunity to fill this gap by displaying the essential elements of LMM within the simplest of contexts, where a comparison with other MVP methods already exists. Hence the purpose of this paper is two fold, to introduce the LMM into the context of structural design methods and, at the same time, demonstrate the methods strong convergence properties.

The outline of the paper is as follow. In section 2 some basic concepts of limit analysis are briefly summarized and the basic formulae for the evaluation of the upper and lower bound collapse multipliers are set up. Moreover, the fundamental assumptions of the LMM to rigid-plastic structures are given. In section 3 the Linear Matching Method is described and convergence is proven in Section 4. The iterative process results in a monotonically reducing upper bound which converges to the exact solution if the linear solutions are evaluated exactly; for finite element solutions the upper bound functional reduces to the least upper bound associated with the class of displacement fields allowed by the FE formulation. In section 5 the method is used to evaluate upper and lower bounds of collapse loads and collapse mechanisms in a single story portal frame structure and the method is given a graphical interpretation. This is followed by an extension of the procedure to multi-story portal frames. These solutions display a

number of interesting convergence properties of the method. At convergence, upper and lower bounds become identical, verifying that the solution is exact. Convergence of the upper bound is generally geometric, the error reducing at each iteration by a constant factor. During the convergence process the upper bound monotonically reduces. The lower bound is observed to generally monotonically increase but, on occasions, can demonstrate a reduction. This is entirely consistent with theory. Final convergence of the upper and lower bounds to a common value can be delayed in cases where two distinctly differing mechanisms exist which give rise to near identical upper bounds. In this case the method can initially converge towards the mechanism with the non-optimal upper bound before then changing to the optimal mechanism. In such cases, lack of full convergence is clearly displayed through the difference between the upper and lower bound.

2. LIMIT ANALYSIS: PROBLEM STATEMENT

In common with all structural systems, portal frames can be analysed within a kinematic framework defined by a set of displacements, in this case the deflections Δ_i^c at the intersection of beams at x_i that are compatible with a set of plastic hinge rotations Φ_j^c at positions h_j . Hence the deformation of the structure is subjected to a severe subclass of all the possible modes of behaviour, those defined by Δ_i^c and Φ_j^c. The equilibrium of bending moments M_j^* with loads F_i^* is then defined by the Galerkin criterion that equilibrium is satisfied if the following virtual work relationships holds for *all* possible sets of Δ_i^c and Φ_j^c;

$$\sum_i F_i^* \Delta_i^c = \sum_j M_j^* \Phi_j^c$$

Let us consider structures composed of a rigid-plastic material which, therefore, has zero displacement up to the collapse load. Mechanism deformations are assumed to be infinitely small so that deflections have no effect on the equations of equilibrium. Reference, moreover, is made to a structure subjected to proportional loading, the intensity of loads being defined by the load factor λ, which is restricted to positive values.

Let the actual plastic collapse load factor of a structure under load be λ_p, and let the collapse mechanism under loads $F_i^* = \lambda_p F_i$ have small hinge rotations Φ_j^p at hinge positions h_j with corresponding plastic moments M_{pj}. The displacements corresponding to the loads $\lambda_p F_i$ in the collapse mechanism are denoted as Δ_i^p.

$$\lambda_p \sum F_i \Delta_i^p = \sum M_{pj} \left| \Phi_j^p \right| \tag{2.1}$$

where since λ_p and $\sum M_{pj} \Phi_j$ are positive, $\sum F_i \Delta_i^p$ is positive.

If the bending moment at position h_j is denoted by M_j, then,

$$-M_{pj} \le M_j \le M_{pj} \tag{2.2}$$

In the following we quote the limit theorems, without proof (see, for example Horne, 1979).

Lower Bound

If, at any load factor λ_{LB}, it is possible to find an equilibrium bending moment distribution M_j^* in equilibrium with the applied loads $\lambda_{LB} F_i$ and everywhere satisfying the yield condition (2.2), then λ_{LB} is either equal to or less than the load factor at failure.

$$\lambda_{LB} \le \lambda_p \,. \tag{2.3}$$

Upper Bound

If, for any assumed plastic mechanism, defined by a set Δ_i^c and Φ_j^c, the external work done by the loads at a positive load factor λ_{UB} is equal to the internal work at the plastic hinges, then λ_{UB} is either equal to or greater than the load factor at failure.

$$\lambda_{UB} \sum_i F_i \, \Delta_i^c = \sum_j M_{pj} \left| \Phi_j^c \right| \quad , \quad \lambda_{UB} \ge \lambda_p \tag{2.4}$$

It is well known that the limit load is uniquely defined although there may well be more than one corresponding mechanism. As the kinematics are defined by a limited class of deformation modes, the limit load so calculated is, strictly, an upper bound and the lower bound defines a lower bound to this upper bound

3. LINEAR MATCHING METHOD FOR LIMIT ANALYSIS

The simple rigid perfectly plastic moment-rotation relation is shown in Figure 1. Perfectly plastic deformation up to indefinitely high rotations is assumed to be possible at the yield moment M_{pj}.

The Linear Matching Method attempts to construct, as the limit of an iterative procedure, linear solutions, $\widetilde{\Phi}_j$ and $\widetilde{M}_j$, for the load λF_i by varying the set of linear moduli R_j:

$$\widetilde{\Phi}_j = \frac{1}{R_j} \widetilde{M}_j \tag{3.1}$$

by a particular scaling factor, discussed below. Equation (3.1) describes an arbitrary sign consistent description of the relationship between the moments, in equilibrium, and compatible rotations which is capable of describing any type of holonomic constitutive assumption. Hence, for any limit state solution there exists a set of R_j, for which the linear solution $\widetilde{M}_j$ is identical to the limit state solution.

The procedure described below provided an iterative procedure which seeks a sequence of values of R_j denoted by R_j^k, so that each solution more closely approaches the correct solution.

Iterative Procedure

We start the procedure with a linear solution for $R_j^0 = R$, a constant and arbitrary λ, producing an initial solution $\widetilde{\Phi}_j^0$ and $\widetilde{M}_j^0$. In the subsequent iterative procedure the moduli R_j^k are adjusted so that a distribution of R_j^{k+1} can be found so that for fixed $\widetilde{\Phi}_j^k$ the moment can be brought to the yield surface, as shown in Figure (1).

i.e. $$\left|\widetilde{\Phi}_j^k\right| = \frac{\left|\widetilde{M}_j^k\right|}{R_j^k} = \frac{M_{pj}}{R_j^{k+1}} \text{ , hence } \quad R_j^{k+1} = \frac{M_{pj}}{\left|\widetilde{M}_j^k\right|} R_j^k \tag{3.2}$$

The quantity $\dfrac{M_{pj}}{\left|\widetilde{M}_j^k\right|}$ is the scaling factor mentioned before.

A new linear solution is now constructed for $R_j = R_j^{k+1}$. The load for this *(k+1)*th solution is chosen by computing the upper bound load parameter λ_{UB}^k corresponding to the previous solution $\widetilde{\Delta}_j^k$ and $\widetilde{\Phi}_j^k$.

At each iteration a corresponding lower bound on the limit load can be found by scaling the moment distribution $\widetilde{M}_j^k$ in equilibrium with $\lambda_{UB}^k F_i$ so that, for the largest possible value of $\lambda = \lambda_{LB}^k$ the scaled moments lie within yield,.

Hence at a particular hinge point,

$$j = m \qquad \frac{\left|\widetilde{M}_m^k\right|\lambda_{LB}^k}{\lambda_{UB}^k} = M_{pm} \tag{3.3}$$

and for

$$j \neq m \qquad \frac{\left|\widetilde{M}_j^k\right|\lambda_{LB}^k}{\lambda_{UB}^k} \leq M_{pj} \tag{3.4}$$

Hence the lower bound is given by:

$$\lambda_{LB}^k = \lambda_{UB}^k \frac{M_{pm}}{\left|\widetilde{M}_m^k\right|} \tag{3.5}$$

Hence, at each iteration, both a lower and an upper bound is determined. In the following section we show that this procedure produces a monotonically reducing sequence of λ_{UB}^k that converges to the least upper bound. At the same time, at convergence, the lower bound equals the upper bound, demonstrating that the converged solution is the exact solution within the class of kinematic fields chosen.

4. CONVERGENCE PROOF

The rotations $\widetilde{\Phi}_j^k$ and displacements Δ_i^k at the k^{th} iteration are used to determine the upper bound λ_{UB}^k via equation (2.4). The subsequent linear solution provides rotations

$\widetilde{\Phi}_j^{k+1}$, displacements Δ_i^{k+1} and a new upper bound λ_{UB}^{k+1}. We now demonstrate that the upper bound load parameter always reduces during this process.

Consider Figure 1 and the following inequality:

$$\int_{\Phi_j^k}^{\Phi_j^{k+1}} \widetilde{M}_j\left(\Phi_j\right) d\Phi_j - \int_{\Phi_j^k}^{\Phi_j^{k+1}} M_{pj} d\left|\Phi_j\right| \geq 0 \tag{4.1}$$

i.e. the area $A \geq 0$. Hence,

$$\frac{1}{2}\widetilde{M}_j\left(\widetilde{\Phi}_j^{k+1}\right)\widetilde{\Phi}_j^{k+1} - \frac{1}{2}\widetilde{M}_j\left(\widetilde{\Phi}_j^{k}\right)\widetilde{\Phi}_j^{k} - M_{pj}\left(\left|\widetilde{\Phi}_j^{k+1}\right| - \left|\widetilde{\Phi}_j^{k}\right|\right) \geq 0 \tag{4.2}$$

where, according to equation (2.4) $\sum M_{pj}\left|\widetilde{\Phi}_j^{k}\right| = \lambda_{UB}^{k} F_i \widetilde{\Delta}_i^{k}$ and $\sum M_{pj}\left|\widetilde{\Phi}_j^{k+1}\right| = \lambda_{UB}^{k+1} F_i\ \widetilde{\Delta}_i^{k+1}$ so inequality (4.2) becomes:

$$\frac{1}{2}\sum_j R_j^k\ \widetilde{\Phi}_j^{k+1^2} - \frac{1}{2}\sum_j R_j^k\ \widetilde{\Phi}_j^{k^2} - \left(\lambda_{UB}^k \sum_i F_i\ \widetilde{\Delta}_i^{k+1} - \lambda_{UB}^k \sum_i F_i\ \widetilde{\Delta}_i^{k}\right) \geq \lambda_{UB}^{k+1} \sum_i F_i\ \widetilde{\Delta}_i^{k+1} - \lambda_{UB}^k \sum_i F_i\ \widetilde{\Delta}_i^{k+1} \tag{4.3}$$

Now the potential energies for the consecutive linear solutions corresponding to stiffnesses R_j^k and R_j^{k+1} are given by:

$$\begin{aligned} \Omega^{k+1} &= \frac{1}{2}\sum_i R_j^k \widetilde{\Phi}_j^{k+1^2} - \lambda_{UB}^k \sum_i F_i\ \widetilde{\Delta}_j^{k+1} \\ \Omega^{k} &= \frac{1}{2}\sum_i R_j^k \widetilde{\Phi}_j^{k^2} - \lambda_{UB}^k \sum_i F_i\ \widetilde{\Delta}_i^{k} \end{aligned} \tag{4.4}$$

Hence inequality (4.4) becomes:

$$\Omega^{k+1} - \Omega^k \geq (\lambda_{UB}^{k+1} - \lambda_{UB}^k)\sum_i F_i \widetilde{\Delta}_i^{k+1} \tag{4.5}$$

The solution of the linear problem with load $\lambda_{UB}^k F_i$ minimizes the potential energy and hence $\Omega^{k+1} \leq \Omega^k$ and, from (4.5),

$$\lambda_{UB}^{k+1} \leq \lambda_{UB}^{\ k} \tag{4.6}$$

Note that equality in (4.6) only occurs when $\widetilde{\Phi}_j^{k+1} = \widetilde{\Phi}_j^{k}$ and $R_j^{k+1} = R_j^k$. Hence λ_{UB}^k defines a monotonically reducing sequence of upper bounds that converge to a solution where $\widetilde{\Phi}_j^{k+1} = \widetilde{\Phi}_j^{k}$. For this solution, at each hinge point two possibilities exist, depending on whether $\widetilde{\Phi}_j^{k+1} = \widetilde{\Phi}_j^{k}$ has a finite value (active hinges) or whether $\widetilde{\Phi}_j^{k+1} = \widetilde{\Phi}_j^{k}$ is infinitesimally small (inactive hinges). For active hinges equation (3.2) gives,

$$\left|\widetilde{\Phi}_j^{k}\right| = \frac{\left|\widetilde{M}_j^{k}\right|}{R_k} = \frac{M_{pj}}{R_{k+1}} \text{ and hence } \left|\widetilde{M}_j^{k}\right| = M_{pj} \tag{4.7}$$

At inactive hinges $\left|\widetilde{M}_j^k\right| \le M_{pj}$. Hence the conditions of both the upper and lower bound theorems are satisfied and the converged solution is the exact solution.

At each iteration the equilibrium moments provide a lower bound λ_{LB}^k which, we now see, becomes equal to the upper bound at convergence. However, it is not possible to prove that the lower bound forms a monotonically increasing sequence. In the examples that follow the lower bound does, generally, monotonically increase but in a few cases reductions do occur. However, the role of the lower bound in determining whether convergence has correctly occurred is essential, as will be demonstrated in the examples.

5. APPLICATIONS

In the following, we investigate the application of this method to the calculation of upper and lower bounds of the limit load for a range of portal framed structures. We begin with a single story frame to fix ideas. This is followed by the solution of multi-story structures, with particular interest in the method's convergence properties.

5.1 Upper and Lower Bounds for a Single Story Frame.

Figure 2 shows a simple portal frame with a fixed base at 1 and 2. The vertical load $V = \alpha H$ and horizontal load $H = \lambda$ remains proportional and defined in magnitude by the load factor λ. The frame is of uniform section with a plastic moment $M_{pj} = M_Y$. When two independent load systems can act simultaneously on a structure in any ratio, it is useful to study the load factors at collapse by means of an interaction diagram, Figure 3 (Horne, 1979). Any line radiating from the origin represents proportional loading and in the following calculations three different values of α are considered: $\alpha = 0.25; 1; 4$.

For problems where concentrated loads are applied, equilibrium requires that maximum and minimum bending moments occur at the ends of uniform beam sections, i.e. at nodes 1 to 2 in Figure 2. Hence plastic hinges may only occur at such nodes and the rotation of local plastic hinges are given by Φ_j, $j = 1$ to $j = 5$ as shown in Figure 4. The exact limit load solution consists of three alternative mechanisms, as shown in Figure 4, giving rise to the interaction diagram of Figure 3.

According to the Linear Matching Method a sequence of linear analyses is undertaken in which the nodal stiffnesses are systematically changed to provide a sequence of upper and lower bounds to the limit load**.** The details of the procedure are given in **Appendix A**. Figures (5 a,b,c) show the evolution of the upper and lower bound values for three values of α, corresponding to different regions of the activation diagram shown in Fig 3.

The evolution of the shape of the collapse mechanism as the solution converges is given in Figures (6 a,b,c), expressed as a function of the parameter $\beta = u/v$, where *u* and *v* are the displacements in the directions of the applied loads as illustrated in Figure 4. The converged mechanism and limit load are consistent with the interaction diagram of Figure 3.

The iteration process is terminated when $\lambda_{UB}^{k} - \lambda_{UB}^{k-1} < 10^{-6}$ and this is achieved in all cases in less than 15 iterations.

5.2 Graphical Representation of the Convergence Process

Convergence of the LMM may be shown through the following graphical representation of the iterative process. At the k[th] iteration the method chooses a stiffness matrix for the next iteration such that: $[M_p] = [R^{k+1}][|\tilde{\Phi}^k|]$, and from the upper bound formula $[M_p][|\tilde{\Phi}^k|] = \lambda_{UB}^{k}[\tilde{\Delta}^k]^T[F_0]$. Now consider the elastic analysis for the (k+1)[th] iteration, for which the magnitude of the applied load is λ_{UB}^{k}. The potential energy of the system for any $[\Phi]$ is given by:

$$\Omega = \frac{1}{2}[\Phi]^T[R^{k+1}][\Phi] - [\Delta]^T \lambda_{UB}^{k}[F_0] \qquad (5.1)$$

so when $\Phi = \tilde{\Phi}^k$, Ω is given by:

$$\Omega(|\tilde{\Phi}^k|) = \frac{1}{2}[M_p]^T[|\tilde{\Phi}^k|] - [\tilde{\Delta}]^T \lambda_{UB}^{k}[F_0] = \frac{1}{2}[\tilde{\Delta}]^T \lambda_{UB}^{k}[F_0] - [\tilde{\Delta}]^T \lambda_{UB}^{k}[F_0] = -\frac{1}{2}[\tilde{\Delta}]^T \lambda_{UB}^{k}[F_0] \qquad (5.2)$$

Hence, a quantity $\bar{\Omega}$ can be defined:

$$\bar{\Omega}([\tilde{\Phi}]) = \frac{\Omega(|\Phi|)}{[\tilde{\Delta}^k]^T[F_0]} + \frac{3}{2}\lambda_{UB}^{k} \qquad (5.3)$$

so that, when $[\tilde{\Phi}] = [\tilde{\Phi}^k]$

$$\bar{\Omega}([\tilde{\Phi}^k]) = \lambda_{UB}^{k} \qquad (5.4)$$

If we now consider the first variation of $\bar{\Omega}$ about this point,

$$\delta\bar{\Omega}(\tilde{\Phi}^k) = \frac{[|\tilde{\Phi}^k|]^T[R^{k+1}][\delta|\Phi|]}{[\tilde{\Delta}^k]^T[F_0]} = \frac{[M_p]^T[\delta|\Phi|]}{[\tilde{\Delta}^k]^T[F_0]} \qquad (5.5)$$

The upper bound load parameter is given by;

$$\lambda_{UB}^{k}([\tilde{\Phi}^k]) = \frac{[M_p]^T[|\tilde{\Phi}^k|]}{[\tilde{\Delta}^k]^T[F_0]} \qquad (5.6)$$

Hence for constant $[\tilde{\Delta}^k]^T[F_0]$

$$\delta\lambda_{UB}\left(\left[\widetilde{\Phi}^{k}\right]\right)=\frac{\left[M_{p}\right]^{T}\left[\delta\Phi\right]}{\left[\widetilde{\Delta}^{k}\right]^{T}\left[F_{0}\right]}=\delta\overline{\Omega}\left(\widetilde{\Phi}^{k}\right) \tag{5.7}$$

This argument demonstrates that the normalized potential energy of the linear problem $\overline{\Omega}$ and the upper bound load factor λ_{UB} coincide at the kth iteration and their local slopes also coincide.

Figure 7 shows λ_{UB} versus the shape of mechanism parameter $\beta = v/u$ for the problem of Figure 2 for the case of $\alpha = 1$. The plot also shows $\overline{\Omega}$ for the $(k+1)^{th} = 11^{th}$ iteration. It can be seen that the matching process chooses a linear material so the upper bound load parameter and the normalised potential energy coincide and are tangential at the k^{th} solution at β^{k}. The $(k+1)^{th}$ solution is obtained as the minimum of the potential energy and use of the resulting rotations provides a lower value of the upper bound. In terms of this graphical representation the convexity conditions (4.1) and (4.2) require that the potential energy curve lies everywhere above the upper bound curve.

Figure 8 shows the same representation as Figure 7 except over a wider range of β and for iterations where the current solution is far from convergence, B, and close to convergence, C. Note that the shape of the potential energy curve depends on the distance from the converged solution. There is a vertex in the limit load plot at the minimum. As a result, an $\overline{\Omega}$ curve which is tangential to the limit load curve close to the vertex must be narrow in order to ensure that it does not cross the upper bound curve. At the vertex, it must collapse onto a vertical line. This is indicative of the fact that there is no rotation at node 2 of Figure 2 for the mechanism associated with the vertex (ie mechanism III of Figure 4). The corresponding linear solution requires that the rotational stiffness of this node is ∞. Any variation of β away from this point requires rotation of this node resulting in a sharp increase in $\overline{\Omega}$. Away from the vertex, where there is rotation and finite stiffnesses at all the nodes, there is a more gradual variation of $\overline{\Omega}$ with β. The mechanism corresponding to point *A* also has zero rotation at one of the nodes (node 3). For the same reason as discussed above, the $\overline{\Omega}$ curve becomes narrow again as this point is approached.

5.3 An estimate of the Rate of Convergence

The rate of convergence of the method depends on both the nature of the particular problem and the choice of the initial set of R_j^0. Note that the value of λ_{UB}^1 is independent of the initial choice of λ and also the absolute magnitude of R. For problems where all the possible hinges are active convergence tends to be rapid. But in the problem just described and those discussed later, there are a significant number of hinges which become inactive in the converged solution. For such hinges, R_j begins with the initial assigned value and increases to much larger values as the solution converges towards the exact value. At each iteration, the value of the corresponding $\widetilde{M}_j^k$ is dominated by equilibrium considerations and remains relatively constant. Hence from (3.1) the corresponding rotation may be expected to reduce by a constant factor and hence the contribution to the upper bound will also reduce by a constant factor. If the convergence of the method were dominated by the reduction of the contribution to the upper bound

made by these inactive hinges, the rate of convergence would be expected to be geometric, i.e. the error reduces by a constant factor over each iteration. If the error in the upper bound at the kth iteration is δ^k,

$$\delta^k = \lambda_{UB}^k - \lambda_{UB}^\infty \ , \tag{5.8}$$

this argument would imply that $\delta^k = \frac{1}{C}\delta^{k-1}$ where C>1 is a constant, an average of the constant values associated with the inactive hinges. Hence

$$\delta^{k+N} = \frac{1}{C^N}\delta^k$$

or

$$\ln \delta^{k+N} = -N \ln C + \ln \delta^k \tag{5.9}$$

Figure 9 shows the logarithm of δ^k versus the iteration numbers for the cases $\alpha = 0.25$, $\alpha = 1$, $\alpha = 4$ as shown in Figure 6 (a,b,c). It can be seen that convergence closely follows equation (5.9) for $\alpha = 0.25$ and $\alpha = 4$ with, in this case $C = 2$, except when the error is extremely small, where numerical rounding errors begin to play a part. For $\alpha = 1$, the initial mechanism for R_j constant is very close to the optimal mechanism and convergence is more rapid.

6. EXTENTION TO MULTI-STORY FRAME STRUCTURES

In this section the extension to multi-story frame structures is discussed to verify the effectiveness of the proposed approach. The procedure is described in detail in Appendix B.

6.1 Three Story Portal Frames

Figure 10 presents the geometry and the sections at which it is necessary to allow for the possible occurrence of plastic hinges of a three story portal frame for a model with 15 elements.

Figure 11 show the exact collapse mechanism, namely a sway in the first two stories and Figure 12 shows the convergence of λ_{UB} and λ_{LB} to the limit load corresponding to this mechanism. Note that the lower bound does not always monotonically increase, but eventually converges to the optimal upper bound. In Figure 13 the rate of convergence is shown where, again, geometric convergence with a slope of ln 2 occurs over most of the iterations. It is interesting to note that the rate of geometric convergence is the same as that shown in Figure 9 for the structure of Figure 2, although there is no theoretical reason why this should be the case.

6.2 A Ten Story Frame

Figure 14 presents the geometry of a ten-story plane frame studied previously by Marin-Artieda and Dargush (2007) where a number of alternative methods were applied. Figure 15 shows the optimal collapse mechanism in the form of an overall sway

mechanism. The convergence process is shown in Figure 16 in terms of values of λ_{UB}, λ_{LB}. The converged values of the bounds and the collapse mechanism are consistent with the exact solution reported by Marin-Artieda and Dargush (2007) where they give a collapse load of 31.3kN for L= 6m and M_y =210kN/m, giving $\frac{\lambda L}{M_y} = 0.894$.

In the same paper, an ABAQUS step by step calculation is reported with a significantly lower collapse load. The reported collection of active hinges at collapse does not form a mechanism and hence no meaningful comparison can be made with this result. The authors place greatest emphasis on the Reduced Elastic Modulus (REM) method of Marriott (1985), which gives a lower bound which tends to converge to a limit load of 30.1kN, 4% less than the exact solution. The REM method gives no indication of the collapse mechanism.

Note that final convergence of the lower bound to the upper bound in Figure 16 takes a significant number of iterations. The rate of convergence is shown in Figure 17 where it can be seen that convergence is initially rapid and geometric so that by 50 iterations the error has reduced to 10^{-8}. There is then about 200 iterations during which the error reduces slowly until, finally, geometric convergence is re-established at the same rate as initially. This behaviour arises from the very close proximity of two mechanisms with near identical collapse loads. The method initially converges towards the mechanism with the higher collapse load before moving over to the optimal mechanism. This phenomenon is best understood in the following example where the two mechanisms are moved further apart by a small change in a plastic modulus.

Consider the case when the plastic moment in beams labelled *f* in Figure 14 is changed by 8% from $M_P(f) = 0.216M_Y$ to $M_P(f) = 0.2M_Y$. In this case the structure has two very distinct collapse mechanisms I and II, shown in Figure 18. Mechanism I consists of a sway of the entire structure with $\lambda_1 = 0.8832$, and for mechanism II only the last seven stories sway, giving $\lambda_2 = 0.8785$. Figure 19 shows the evolution of the two bounds with increasing number of iterations. The upper bound shows a rapid convergence to mechanism I, followed by a very slow convergence to the optimal mechanism II where the upper and lower bounds coincide. The initial apparent convergence to mechanism I is shown to be false by the remaining large difference between the upper and lower bounds. Full convergence requires a large number of iterations; in excess of 500.

It is evident from Figure 20 that the convergence is geometric in the early stages as the deformed shape converges towards mechanism I and again in the latter stages as mechanism II is approached, but it is much slower in-between as the solution process seeks out the new mechanism.

It is clear that the existence of distinct mechanisms with near equal collapse load limits can delay eventual convergence to the optimal mechanism. The fact that the upper and lower bound do not coincide after the initial convergence process clearly indicates that this phenomenon has occurred and the lower bound will certainly be less at this stage than the eventual converged upper bound. In the following we ask the question: how close do collapse loads for adjacent mechanisms have to be for this phenomenon to occur. Consider again the structure and plastic moments shown in Figure 14. To answer this question, the values of the plastic moments for elements a(*), b(*), c(*) in Figure 21 are changed by an amount α, such that $M_p^{NEW} = \alpha M_P$. Over the range $0.25 \le \alpha \le 2$ three possible optimal mechanisms occur, as shown in Figure 22. The converged values

of lambda are compared in Figure 23b with the upper bounds associated with the three mechanisms (see Appendix C), showing that a change in the optimal mechanism occurs at $\alpha = 0.5$ and $\alpha = 1.05$. Figure 23a shows the number of iterations to convergence over the entire range of α, which is assumed to occur when $\lambda_{UB}^{k} - \lambda_{UB}^{k-1} < 10^{-6}$

For this very precise criterion of convergence, it can be seen that large numbers of iterations are only required when there are two mechanisms with upper bounds that are very close to each other. The load factors for mechanism 1 and mechanism 2 coincide when $\alpha = 1$. For $\alpha < 1$ and $\alpha > 1.05$ convergence occurs in the order of 100 iterations. For $1 < \alpha < 1.05$ the load factors for the two competing mechanism differ by, at most 2%.

7. CONCLUSIONS

The Linear Matching Method provides a programming method for the evaluation of limits in classical plasticity that differs significantly from other programming methods. Although it is best described as a convergent upper bound method, each iteration provides an equilibrium set of moments as well as a compatible set of kinematic variables. Hence both upper and lower bounds are generated which, at convergence, coincide and verifying that the exact solution has been obtained. This property is unique to the Linear Matching Method.

This paper has concentrated on the convergence properties of the method applied to rigid plastic portal frames. We find convergence tends to be geometric and reasonably rapid. We also find that the close proximity of upper bounds to the optimal mechanism can delay convergence, by the method first seeking out the mechanism associated with the non-optimal solution before then slowly converging to the optimal solution. It would appear that this phenomenon will only occur if the distributions of hinges in the two mechanisms are very distinct and the upper bounds very close together. The existence of the phenomenon in a particular problem is clearly displayed through the difference between the upper and lower bound.

The inherent simplicity of the method by using, as its basis, linear analysis, together with its strong convergence properties, encourages the view that it is a method that may usefully be seen alongside classical programming approaches to structural design.

ACKNOWLEDGEMENTS

O.B. would like to acknowledge support from the University ‘Mediterranea’ of Reggio Calabria to visit the University of Oxford, during which period this research was conducted.

Appendix A- Linear matching method for single story frame- Matrix Formulation

The Linear Matching Method involves performing a sequence of linear analyses by systematically varying the stiffness, to provide a sequence of upper and lower bounds to the limit load. The details of the procedure are reported in this appendix. Let us assign a rotational stiffness R_i at each plastic hinge $\widetilde{\Phi}_j$ and the related moments are given by: $\left[\widetilde{M}\right]=[R]\left[\widetilde{\Phi}\right]$ where $\left[\widetilde{M}\right]$ is a bending moment vector, $[R]$ is the diagonal matrix of rotational stiffnesses, where

$$\left[\widetilde{M}\right]=\begin{bmatrix}\widetilde{M}_1\\ \widetilde{M}_2\\ \widetilde{M}_3\\ \widetilde{M}_4\\ \widetilde{M}_5\end{bmatrix},\ [R]=\begin{bmatrix}R_1 & 0 & 0 & 0 & 0\\ 0 & R_2 & 0 & 0 & 0\\ 0 & 0 & R_3 & 0 & 0\\ 0 & 0 & 0 & R_4 & 0\\ 0 & 0 & 0 & 0 & R_5\end{bmatrix} \text{ and } \left[\widetilde{\Phi}\right]=\begin{bmatrix}\widetilde{\Phi}_1\\ \widetilde{\Phi}_2\\ \widetilde{\Phi}_3\\ \widetilde{\Phi}_4\\ \widetilde{\Phi}_5\end{bmatrix}=[B]\left[\widetilde{\Delta}\right] \tag{A.1}$$

Here $[\Delta]=\begin{bmatrix}u\\ v\end{bmatrix}$ is the vector of independent degrees of freedom and [B] is the shape function matrix:

$$[\mathbf{B}]=\begin{bmatrix}1/L & 0\\ 1/L & -1/L\\ 0 & 2/L\\ 1/L & 0\end{bmatrix} \textit{ and } [\Delta]=\begin{bmatrix}u\\ v\end{bmatrix} \tag{A.2}$$

With the load vector ;

$$[F]=\lambda\begin{bmatrix}H_0\\ V_0\end{bmatrix}=\lambda[F_0] \tag{A.3}$$

the total potential energy for the (k+1)th linear solution is given by:

$$\Omega=\frac{1}{2}\left[\widetilde{\Phi}^{k+1}\right]^T[R_k]\left[\widetilde{\Phi}^{k+1}\right]-\lambda_{UB}^k\left[\widetilde{\Delta}^{k+1}\right]^T[F_0]=\frac{1}{2}\left[\widetilde{\Delta}^{k+1}\right]^T[K_k]\left[\widetilde{\Delta}^{k+1}\right]-\lambda_{UB}^k\left[\widetilde{\Delta}^{k+1}\right]^T[F_0] \tag{A.4}$$

where $[K_{k+1}]=[B]^T[R_{k+1}][B]$ denote the stiffness matrix. The linear problem is solved by minimizing the potential energy, i.e.

$$[K_{k+1}]\left[\widetilde{\Delta}^{k+1}\right]=\lambda_{UB}^k[F_0]$$

At each independent node the rotations are related to the independent displacement vector $[\Delta]$ by (A.1).

Upper Bound Evaluation

For a particular load ratio α the vector of external loads can be written as follow:

$$[F]=\begin{bmatrix} H \\ V \end{bmatrix}=\lambda\begin{bmatrix} H \\ \alpha H \end{bmatrix}=\lambda[F_0] \tag{A.5}$$

For any compatible mechanism from the upper bound formula eq. (2.3):

$$\lambda_{UB}\left[\tilde{\Delta}\right]^T[F_0]=\sum_{j=1}^{5} M_Y\left|\tilde{\Phi}_j\right| \tag{A.6}$$

For this particular case Φ_i's can defined so that they are always positive, see Figure 4; and hence

$$\lambda_{UB}\left[\tilde{\Delta}\right]^T[F_0]\le\sum_{j=1}^{5} M_Y[I]^T[B]\left[\tilde{\Delta}\right] \tag{A.7}$$

where the vector $[I]$ is a unit matrix.
The upper bound load multiplier from equation (A.6) is then given by :

$$\lambda_{UB}=\frac{\sum_{n=1}^{5} M_Y[I]^T[B]\left[\tilde{\Delta}\right]}{\left[\tilde{\Delta}\right]^T[F_0]} \tag{A.8}$$

Briefly, the main steps for determinig the upper bound using the LMM are:

1) The first linear analysis is made with $R_{i=1,5}=1$ and $\lambda_{UB}=1$.

2) The rotational stiffness R_i at each node is adjusted according to the rules of LMM so that at iteration k+1 the new distribution of rotational stiffness is :

$$R_j^{k+1}=R_i^k\left(\frac{M_Y}{\left|\tilde{M}_j^k\right|}\right)$$

3) A new linear analysis is performed with the new stiffness matrix R_j^{k+1} so a new displacement vector $\left[\tilde{\Delta}\right]$ and $\left[\tilde{\Phi}\right]=[B]\left[\tilde{\Delta}\right]$ and λ_{UB}^k can be evaluated and $[F]=\lambda_{UB}^k[\alpha]$ is the load for the next iteration.

The process is iterated until the lowest upper bound is reached. The lower bound is given by eq. (3.5):

$$\lambda_{LB}^k=\lambda_{UB}^k\frac{M_Y}{\max\limits_j\left|\tilde{M}_j^k\right|} \tag{A.9}$$

Appendix B- Matrix formulation for multistory frame

Let us consider a single beam element (Fig.B1a) with hinge positions at its ends adjacent but distinct from nodes *i* and *j* where the beam is connected to other beams. As before Φ_i denotes the hinge rotation and the rotation of the nodes is separately denoted by ϑ_i. The displacements of the nodes parallel to and perpendicular to the beam length are denoted by u_i, v_i respectively.

For rotation of hinges with no rotation of nodes, Figure B1b :

$$\Phi_i = \frac{v_j - v_i}{L};\ \Phi_j = \frac{v_j - v_i}{L} \tag{B.1}$$

and Fig.B1c shows the rotation of hinges due to rotations of nodes :

$$\Phi_i = -\vartheta_i;\ \Phi_j = -\vartheta_j \tag{B.2}$$

Hence the total rotation of the hinges is the sum of these (B.1) and (B.2):

$$\Phi_i = \frac{v_j - v_i}{L} - \vartheta_i;\ \Phi_j = \frac{v_j - v_i}{L} - \vartheta_j \tag{B.3}$$

The element is considered inextensible and hence the beam extension:

$$e = u_i - u_j = \text{constant}$$

Hence for a typical element the vector $[\Phi]$ of the local hinge rotations and beam extension is related to the element displacement vector $[u]$ of nodal displacements and rotations as follow:

$$[\Phi] = \begin{bmatrix} \Phi_i \\ \Phi_j \\ e \end{bmatrix} = \underbrace{\begin{bmatrix} 0 & -1/L & -1 & 0 & 1/L & 0 \\ 0 & -1/L & 0 & 0 & 1/L & -1 \\ L & 0 & 0 & 0 & L & 0 \end{bmatrix}}_{[C]} \underbrace{\begin{bmatrix} u_i \\ v_i \\ \vartheta_i \\ u_j \\ v_j \\ \vartheta_j \end{bmatrix}}_{[u]} = [C][u] \tag{B.4}$$

where $[C]$ is the compatibility matrix. In turn the element displacement vector $[u]$ is related to a global matrix of global degrees of freedom $[U]$ by the matrix $[\Psi]$,

$$[u] = [\Psi][U]$$

Hence $$[\Phi] = [B][U] \quad \text{where } [B] = [C][\Psi]$$

The stiffness matrix for each element is now:

$$[K]_{el} = [B]^{T'}[R][B] \quad \text{where} \quad [R] = \begin{bmatrix} R_i & & \\ & R_j & \\ & & E_l \end{bmatrix}$$

Where E_L is the elongation stiffness, given a suitable large value; in our calculations $E = 1.10^6$.

The solution of the linear problem for a particular set of $[R]$ is, therefore, given by,

$$[K][\tilde{U}] = \lambda_{UB}[F_0] \quad \text{where} \quad [K] = \sum_{el}[K]_{el} \tag{B.5}$$

The rotation at plastic hinges and the upper bound load parameter can be evaluated from the following relations:

$$[\tilde{\Phi}] = [B][\tilde{U}] \tag{B.6}$$

$$\lambda_{UB}[\tilde{U}]^T[F] = \sum_{hinges} M_{pj}|\tilde{\Phi}_j| \tag{B.7}$$

Now according to the procedure we can adjust iteration by iteration the rotational stiffness at each hinge R_j^k:

$$R_j^{k+1} = \frac{M_{yj}}{|\tilde{\Phi}_j^k|} \tag{B.8}$$

So with the new $[R^{k+1}]$ matrix the $[K]$ matrix can be reconstructed. We solve (B.5) and can determine the new rotations from (B.6) and the new upper bound from (B.7), so:

$$\lambda_{UB} = \frac{\sum_{hinges}|\Phi_j|M_{pj}}{[U]^T[F_0]} \tag{B.10}$$

The lower bound can be evaluated from the upper bound from equation (3.5)

Appendix C- Upper Bound for frame of Figure 21

In Fig.22 three different values of the collapse load multiplier can be determined assuming the 3 collapse mechanisms.

For the first mechanism :

Work done: $\lambda_1 \cdot 27.5 \cdot L\not{\theta} = \not{\theta} M_Y \left[\alpha\left(0.85+2+0.85+12\right)+12\cdot 0.45+16\cdot 0.2\right]$

ie. $$\frac{\lambda_1 L}{M_Y} = \frac{\alpha 15.7+8.6}{27.5} \qquad \text{(C.1)}$$

For the second mechanism:

Work done: $\lambda_2 \cdot 14 \cdot L\not{\theta} = \not{\theta} M_Y \left(0.85+2+0.85+12\cdot 0.45+16\cdot 0.2\right)$

ie. $$\frac{\lambda_2 L}{M_Y} = 0.87857 \qquad \text{(C.2)}$$

For the third mechanism :

Work done: $\lambda_3 \cdot L\not{\theta} \cdot \left(3+7\cdot\frac{3}{2}\right) = \not{\theta} M_Y \left[\alpha\left(4\cdot 0.85+2\cdot 2+8\cdot 1\right)\right]$

ie. $$\frac{\lambda_3 L}{M_Y} = \frac{\alpha 30.8}{27} \qquad \text{(C.3)}$$

7. REFERENCES

Ainsworth R.A. Ed, R5: Assessment Procedure for the High Temperature Response of Structures, Issue 2, Nuclear Electric (now British Energy),Barnwood Laboratories, Gloucestershire, 1997 UK.

Chen H. F., Ponter A. R. S. and Ainsworth R. A., 2006-a, "The linear matching method applied to the high temperature life assessment of structures. Part 1. Assessments involving constant residual stress fields", Int. Jn. of Pressure Vessels and Piping, 83, 123-135.

Chen H. F., Ponter A. R. S. and Ainsworth R. A., 2006-b, "The linear matching method applied to the high temperature life assessment of structures. Part 2. Assessments beyond shakedown involving changing residual stress fields", Int. Jn. of Pressure Vessels and Piping, 83, 136-147.

Cocchetti G., Maier G., 2003 "Elastic–plastic and limit-state analyses of frames with softening plastic-hinge models by mathematical programming", International Journal of Solids and Structures, 40, 7219–7244.

Ferris M.C. and Tin-Loi F., 2001 Limit analysis of frictional block assemblies as a mathematical program with complementarity constraints, International Journal of Mechanical Sciences 43:209-224.

Horne M.R., 1979. Plastic theory of structures. Pergamon Press,.UK

Mackenzie D. and Boyle T., 1993 "A method of estimating limit loads by iterative elastic analysis.I simple example, Int.J.Pres.Ves. Piping 53, 77.

Marin-Artieda C.C., Dargush G.F. 2007 "Approximate limit load evaluatio of structural frames using linear elastic analysis", Engineering Structures 29, 296-304.

Marriott D.L., 1985, "Evaluation of deformation on load control of stresses under inelastic conditions using elastic finite element stress analysis, ASME Pressure Vessels and Piping Conference, 1985,Pittsburg, in: R.Seshadri et al., eds., Codes and Standards and Applications for design and Analysis of Pressure Vessel and Piping Components", ASME PVP 136, 1988, 3.

Ponter A.R.S., 2007, "The Linear Matching Method for the Evaluation of Limit

Loads, Shakedown Limits and Related Problems", Variational Formulations in

Mechanics in Theory and Applications, Ed Taroco E., de Souza Neto and Novotny,

CIMNE, Barcelona,Spain, 243-262.

Ponter A.R.S. and Engelhardt M , 2000 "Shakedown Limits for a General Yield Condition: Implementation and Examples for a Von Mises Yield Condition", European Journal of Mechanics, A/SolidsVol.19, No3, 423-446.

Ponter A.R.S., Fuschi P. and Engelhardt M., 2000 "Limit Analysis for a General Class of Yield Conditions", European Journal of Mechanics, A/Solids, Vol 19, No3, 401-422.

Seshadri R., Fernando C., 1993 "Limit loads of framed structures and arches using the GLOSS R-node method. Transactions of the ASME,; 17(2): 197-214.

Tangaramvong S. and Tin-Loi F., 2007 Limit analysis of strain softening steel frames under pure bending, Journal of Constructional Steel Research 63: 1151-1159. Tangaramvong S. and Tin-Loi F., 2008 Simultaneous ultimate load and deformation analysis of strain softening frames under combined stresses, Engineering Structures 30: 664-674.

Weichert D. and Maier G. Eds, 2001., Inelastic Behaviour of Structures under Variable Repeated Loading – Direct Analysis Methods, , International Centre for Mechanical Sciences Lecture No 432, Springer-Verlag.

Figure Captions

Figure.1 Graphical interpretation of matching procedure at increment *k+1.*

Figure 2 A single story portal frame.

Figure 3 Interaction diagram for the structure of Figure 1 (Horne, 1979).

Figure 4 Possible collapse mechanisms for the structure of Fig 2. The number of each node is given in Fig.2.

Figure 5 Evolution of the upper and lower bounds for (a) $\alpha = 0.25$, (b) $\alpha = 1$ and (c) $\alpha = 4$.

Figure 6 Evolution of the shape of the collapse mechanism for (a) $\alpha = 0.25$, (b) $\alpha = 1$ and (c) $\alpha = 4$.

Figure 7 Graphical Representation of the convergence process for the $k=10^{th}$ iteration.

Figure 8 The variation of $\bar{\Omega}$ at different stages of the convergence process.

Figure.9 Rate of convergence for $\alpha = 0.25$, $\alpha = 1$ and $\alpha = 4$. The plot shows geometric convergence ($\alpha = 0.25$, $\alpha = 1$) except when the error is extremely small.

Figure.10 Three story portal frame analysed in section 6.1. The plastic moment of each beam element is indicated on the figure.

Figure 11 The collapse mechanism observed in the analysis of the structure in Fig 10.

Figure 12 Evolution of the upper and lower bound for the structure in Fig 10.

Figure.13 Rate of convergence shows approximately geometric convergence.

Figure.14 Ten-story frame. The plastic moments assumed in the initial analysis of section 6.2 are indicated adjacent to each beam element,

Figure.15 Collapse mechanism for the ten-story frame of Fig 14.

Figure.16 Evolution of the upper and lower bound related to Fig.15.

Figure.17 Rate of convergence initially rapid and geometric (the error has reduced to 10^{-8}) then the error reduces slowly until, finally, geometric convergence

Figure 18 The collapse mechanisms observed in the analysis of the structure shown in Fig 14.

Figure 19 Evolution of upper and lower bounds for the structure of Fig14, showing the initial rapid convergence towards the limit load corresponding to mechanism I followed by a slower convergence to the exact limit load corresponding to mechanism II

Figure.20 Rate of convergence shows a rapid and geometric convergence to the first upper bound and then a slower convergence to the second upper bound

Figure. 21 Structure in Fig14 with a range of plastic moment values given by $M_p^{NEW} = \alpha M_p$.

Figure.22 Optimal collapse mechanism over a Range $0.25 \le \alpha \le 2$.

Figure 23 (a) Number of iterations for convergence as a function of the strength parameter α (b) Limit loads for each of the mechanism shown in Fig 22, showing the range of dominance of each mechanism.

Figure A1 Nodal rotations.

Figure B1 (a) Beam element from nodes *i* and *j* , (b) Beam with no rotation of nodes, (c) beams with the rotation of hinges due to rotations of nodes.

Fig.1

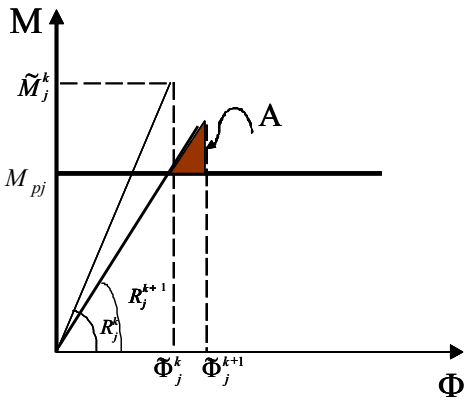

Fig.2

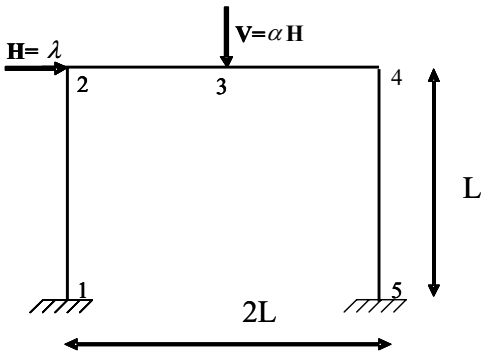

Fig.3

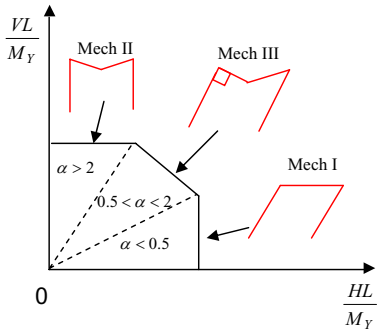

Fig.4

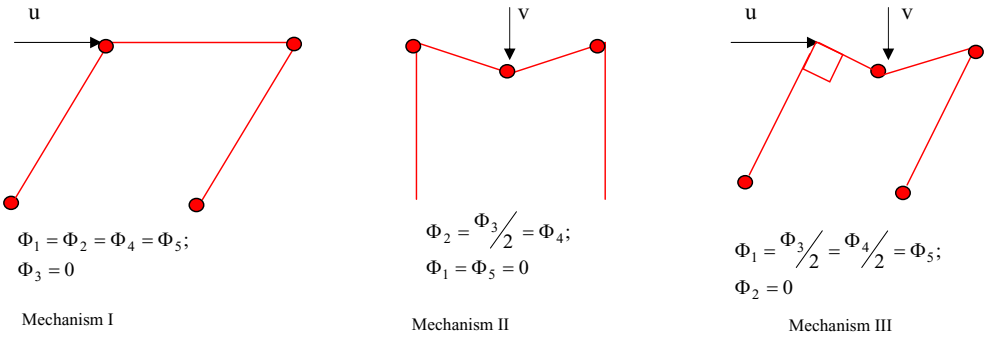

Mechanism I

Mechanism II

Mechanism III

Fig.5a, b, c

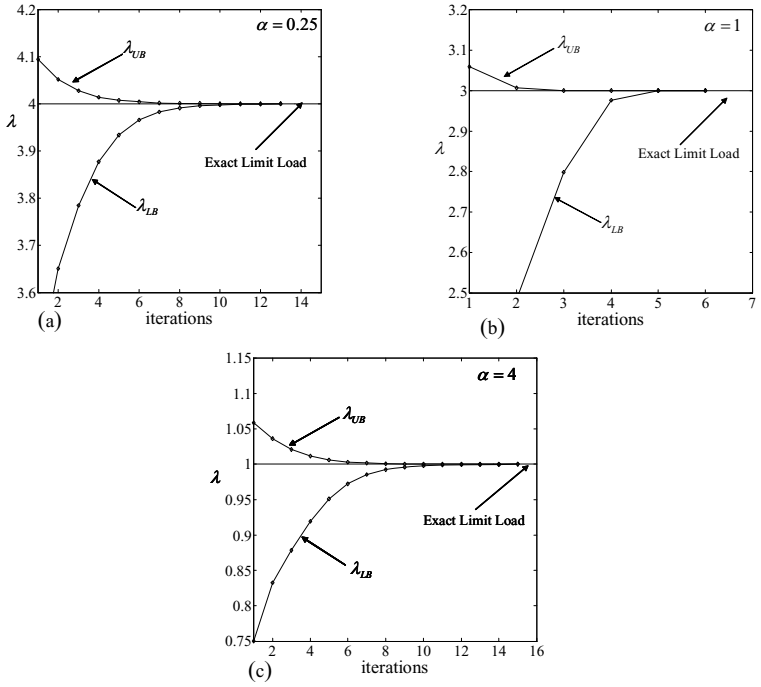

Fig.6a, b, c

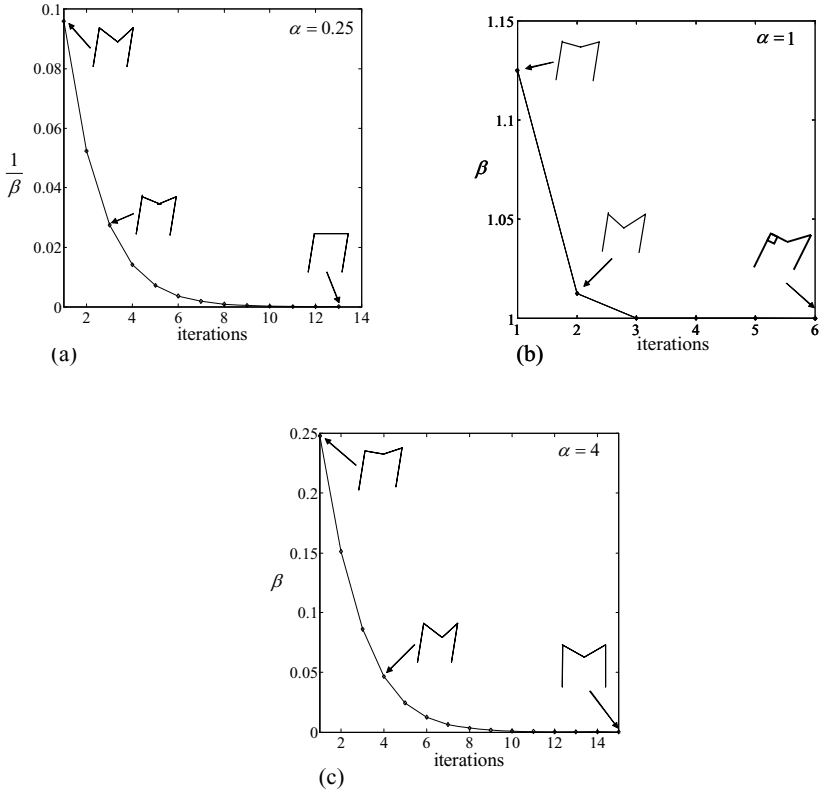

Fig.7

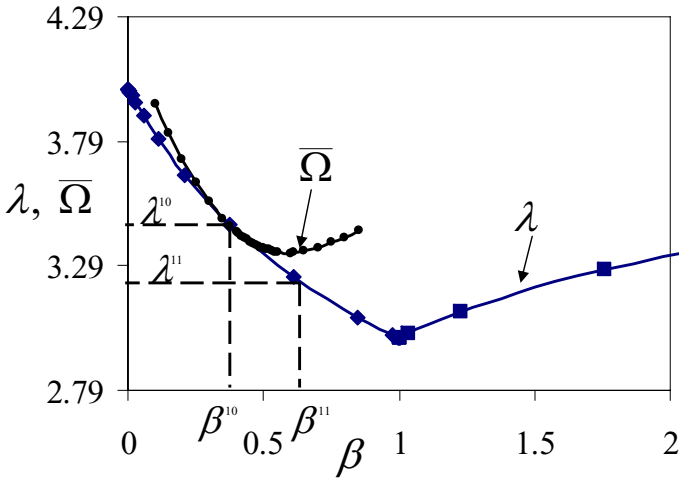

Fig.8

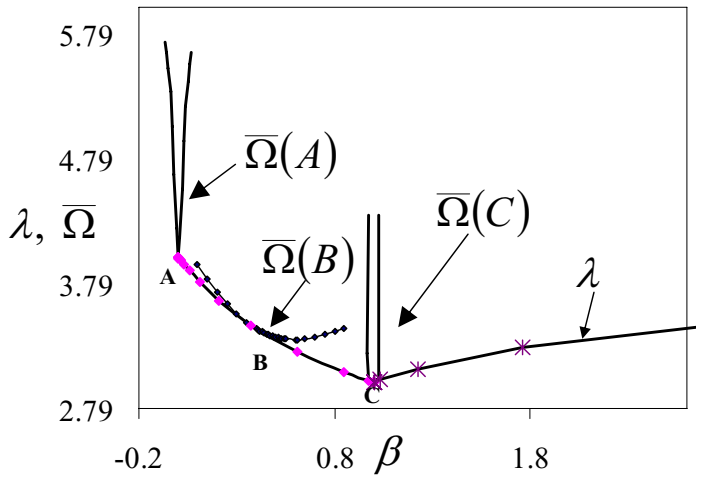

Fig.9

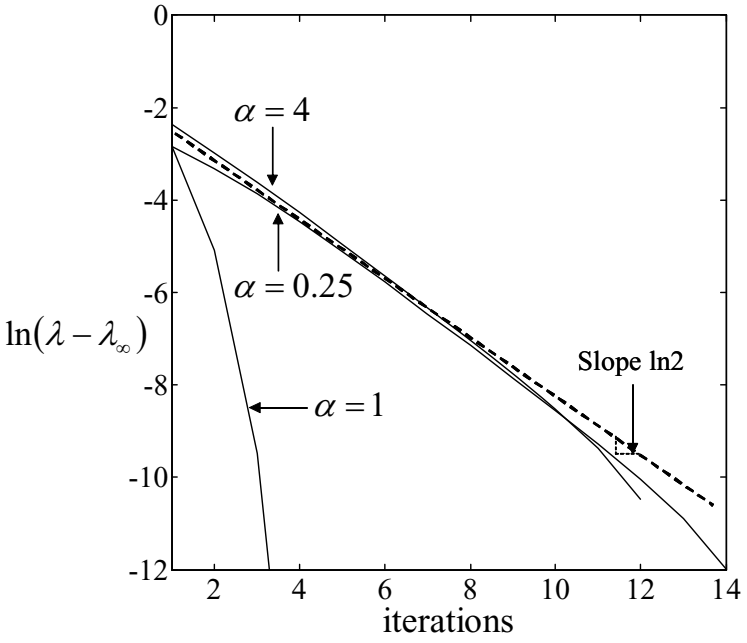

Fig.10

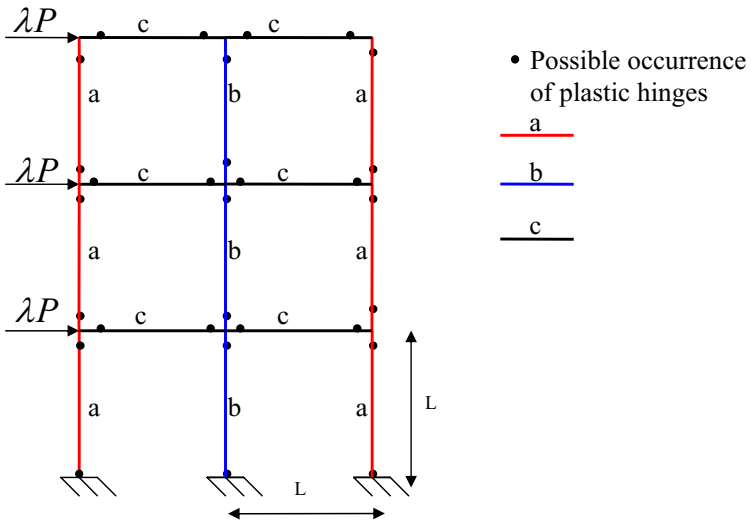

Fig.11

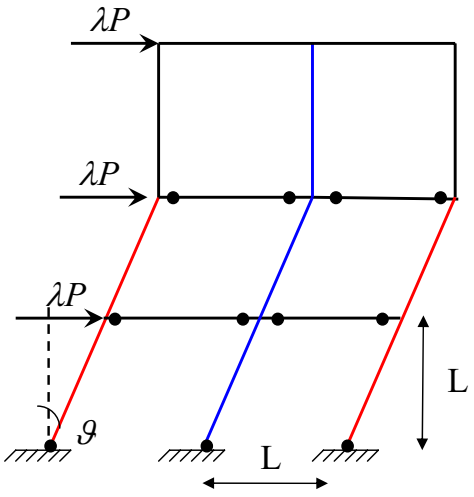

- Plastic hinges

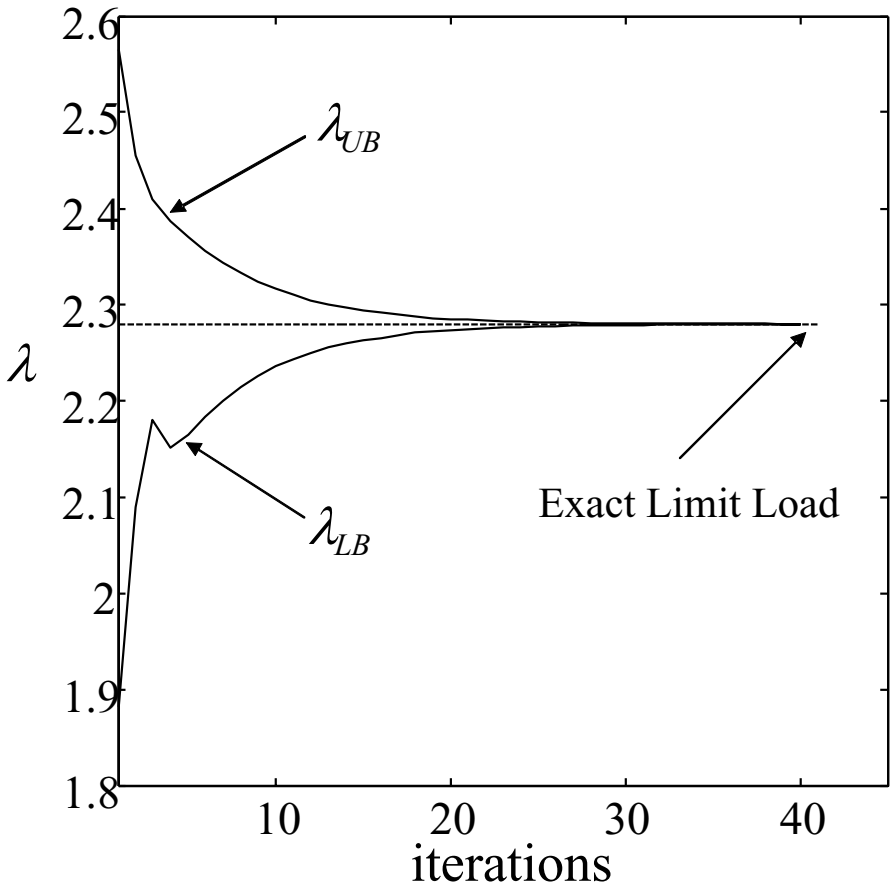

Fig.12

Fig.13

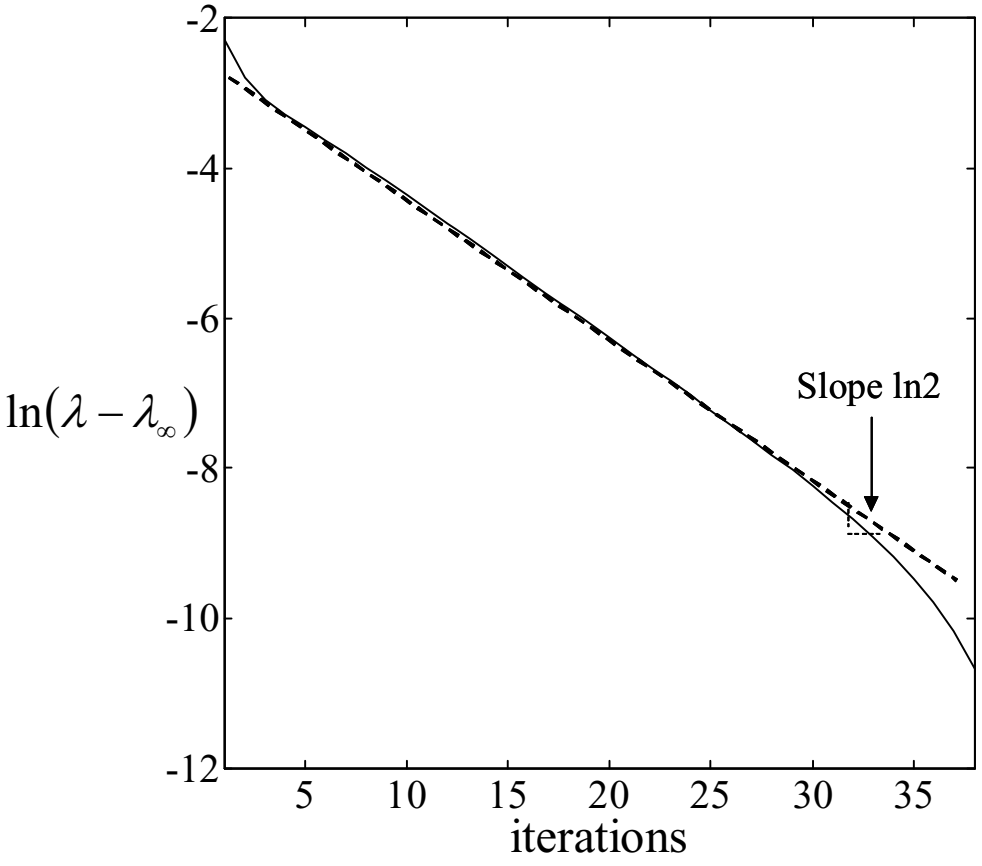

Fig.14

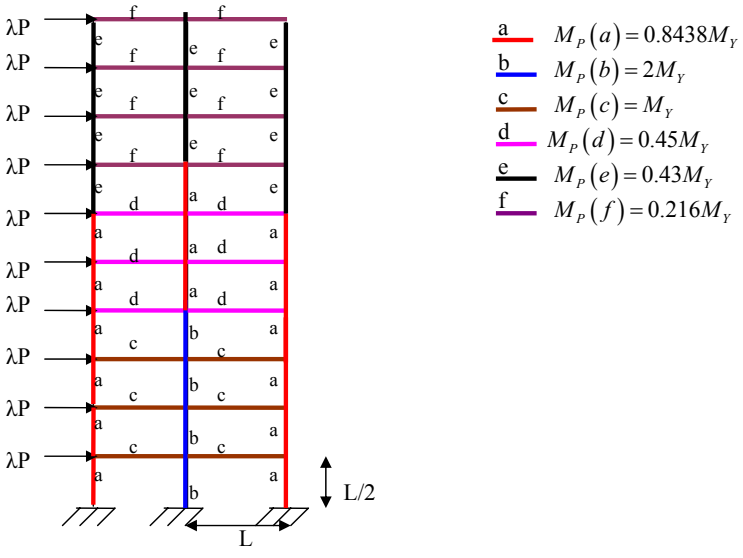

Fig.15

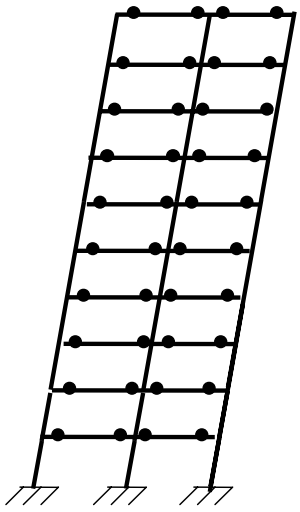

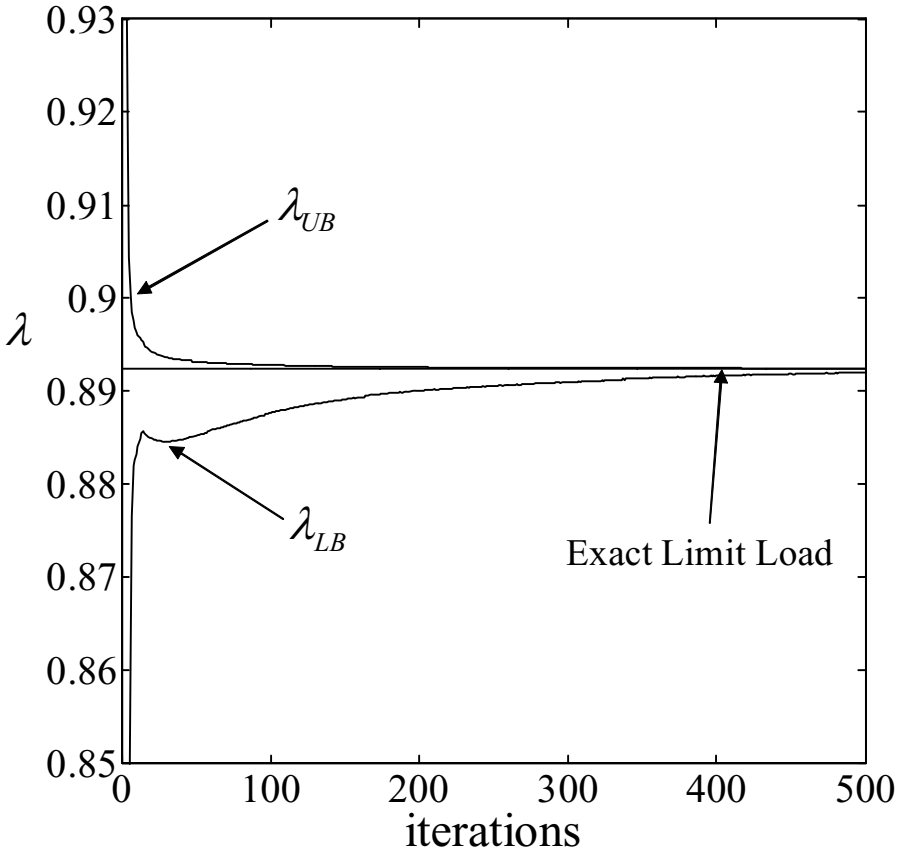

Fig.16

Fig.17

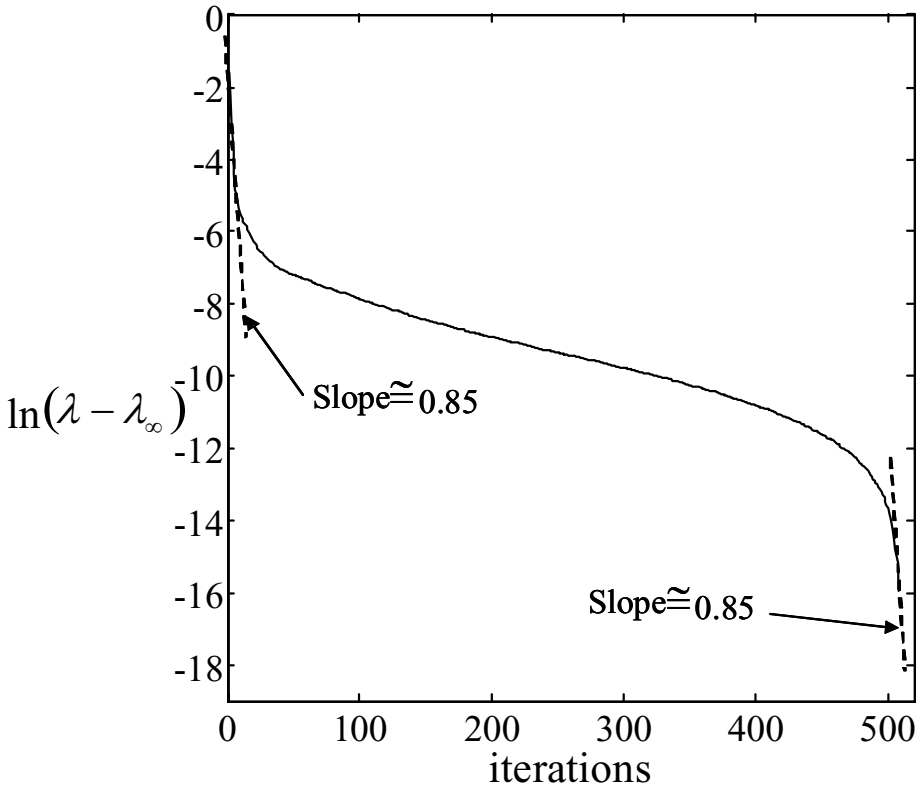

Fig.18

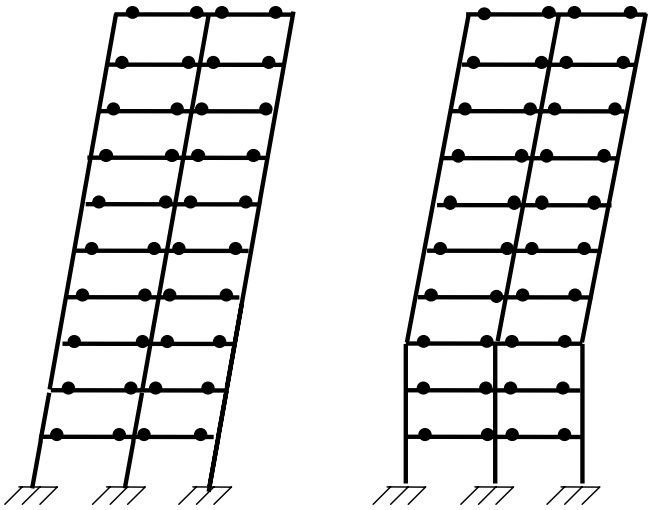

Mechanism I Mechanism II

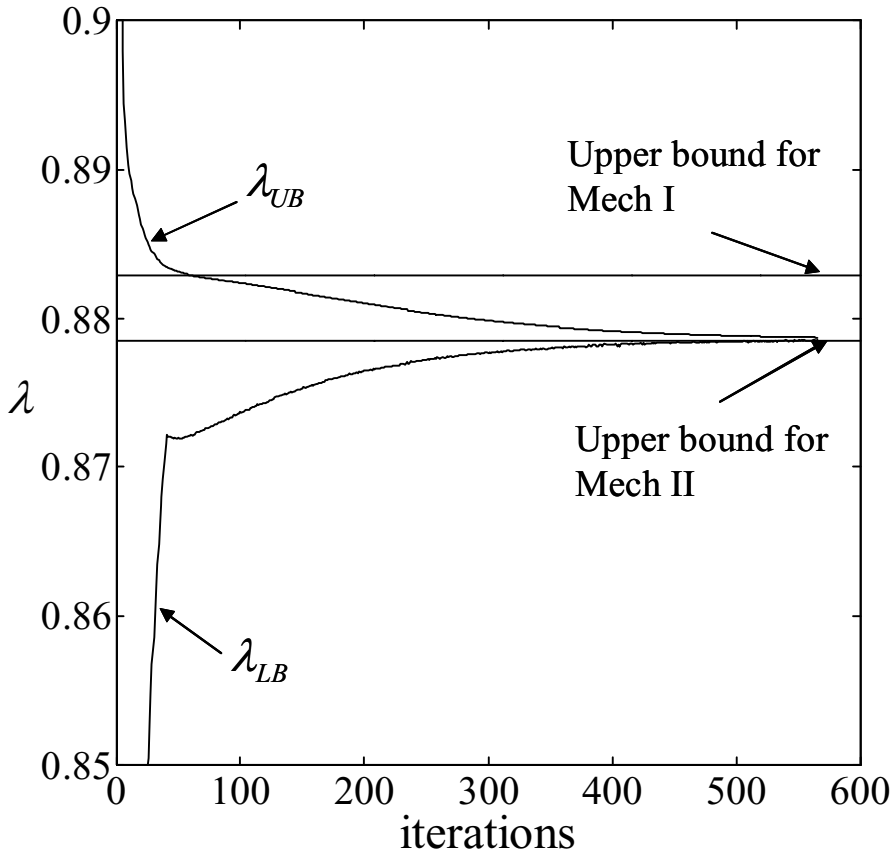

Fig.19

Fig.20

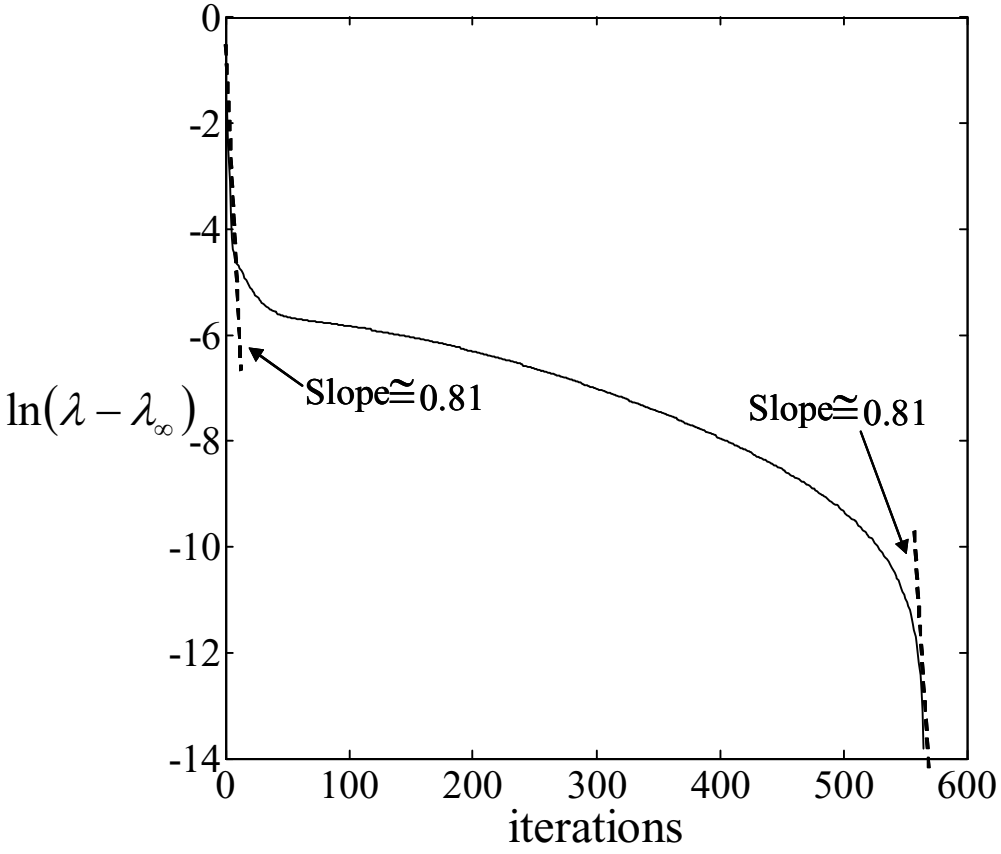

Fig.21

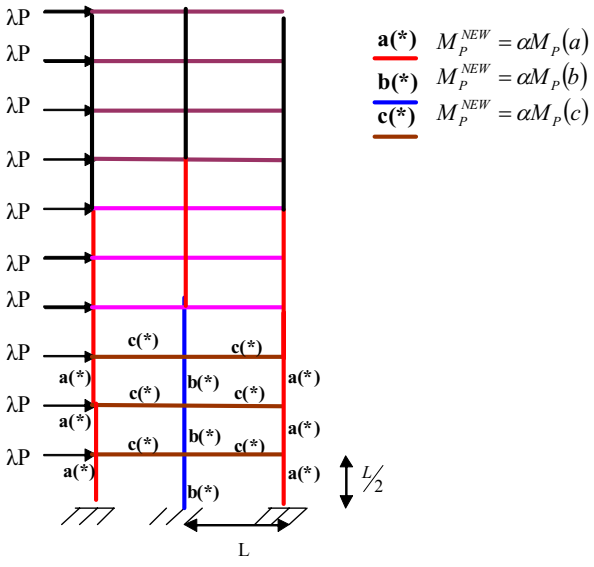

Fig.22

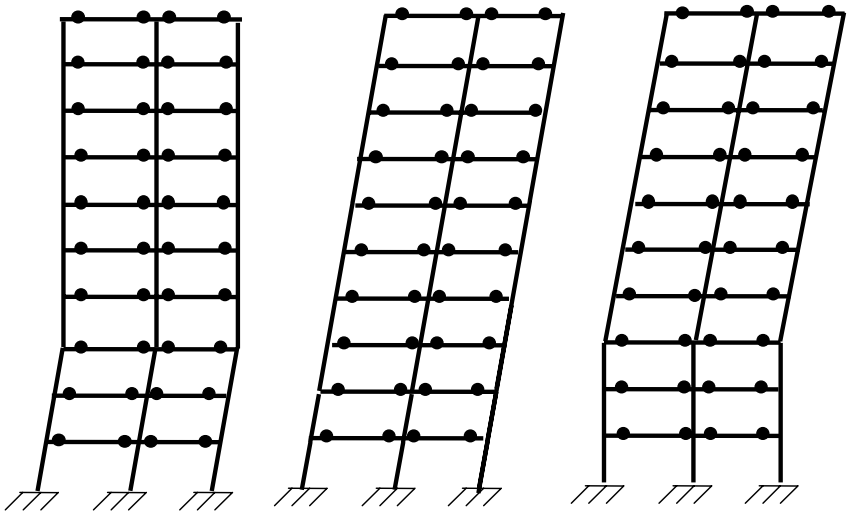

Mechanism I Mechanism II Mechanism III

Fig.23a, b

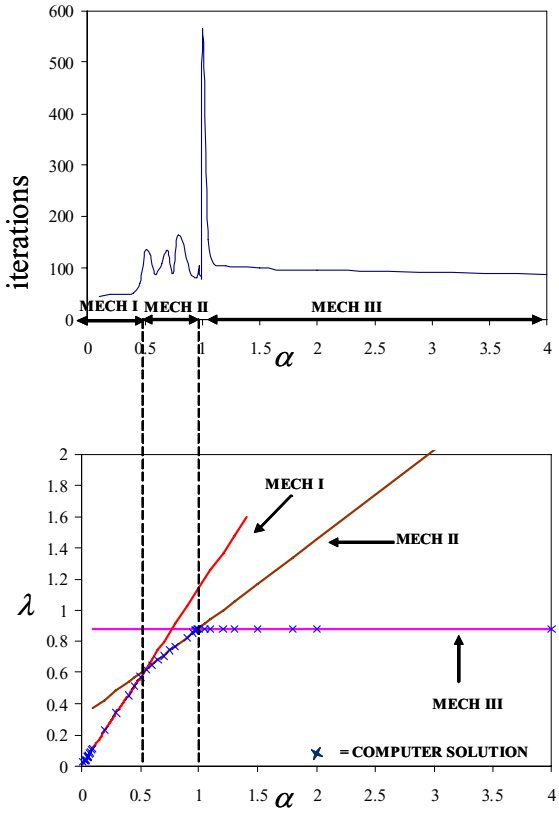

Fig A1

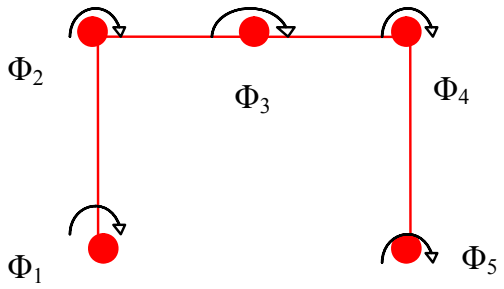

Fig B1

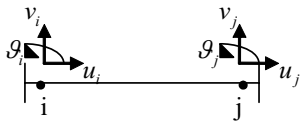

(a)

$u_i = u_j$

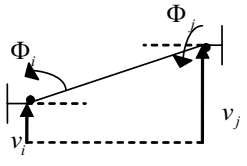

(b)

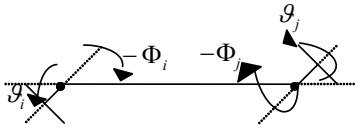

(c)